Enhancing the Electrochemical Performance of Blended Single-Ion Conducting Polymers by Smart Modification of the Polymer Structure

Gerrit Michael Overhoff [1], Elisabeth Verweyen [1], Philipp Roering [1], Martin Winter [1,2], Gunther Brunklaus [1,]*

[1] Forschungszentrum Jülich GmbH, Helmholtz Institute Münster, IEK-12, Corrensstr. 46, 48149 Münster, Germany

[2] MEET Battery Research Center, Institute of Physical Chemistry, University of Münster, Corrensstr. 46, 48149 Münster, Germany

KEYWORDS: lithium metal battery; single-ion conducting polymer; NMC; plasticizer distribution; gel polymer; polymer blend

ABSTRACT: Single-lithium ion conducting polymers represent a promising class of electrolytes that potentially enable the utilization of lithium metal anodes in next-generation batteries. The immobilization of anions within the polymer's structure in principle mitigates issues related to localized ion depletion, resulting in decreased cell polarization when compared to common dual-ion conductors comprising poly(ethyleneoxide) and lithium salt. However, the intrinsic rigidity of these materials often necessitates an incorporation of flowable components

and blending with other polymers, such as PVdF-HFP, to enhance the mechanical flexibility of the resulting polymer membranes. Within polymer blends, distinct phases may be present and the distribution of plasticizers among these phases is highly crucial, as they act as carrier molecules for Li^+ transport. In this study, we thus explored the impact of polymer chain modification from a rigid aromatic single-ion conducting polymer to a more flexible polymer by introducing ethyleneglycol units into the backbone. Notably, this alteration yielded a substantial decrease of 100 °C of the glass transition temperature and a sixfold increase in ionic conductivity (0.5 mS cm^{-1} @ 40 °C) after blending with PVdF-HFP and addition of EC:DMC. Atomistic molecular dynamic simulations suggest that this enhancement can be attributed to a high concentration of plasticizer within the Li^+ containing phase. In symmetric Li||Li cells, exceptional performance was achieved, demonstrating operation at high limiting current density and successful plating/stripping for 1000 hours at 0.2 mA cm^{-2}. When paired with high-voltage NMC cathodes, the introduced polymer structures exhibited noteworthy capacity retention after 800 cycles, emphasizing advantages brought forth by flexible and adapted polymer architecture.

1. **INTRODUCTION**

Electrification of the mobility sector is currently driving research efforts to afford cell designs for high-energy density applications. Lithium (Li) metal anodes comprise a highly promising approach, benefitting from its gravimetric and volumetric capacity,[1] though in practice challenges such as inhomogeneous lithium metal deposition impairs large-scale implementations.[2] Polymer electrolytes are mechanically robust materials that potentially could withstand lithium protrusion, also enabling sufficient electrode contacts while being readily processable.[3,4] Despite commercialization by Bollore,[5] the to date most recognized type of electrolyte, poly(ethylene)oxide (PEO), suffers from insufficient ionic conductivity at temperatures below 60°C and challenges from cell polarization at higher current densities.[6,7] In view of charge carrier transport, lithium ion transference numbers (t_{Li+}) below 0.5 are correlated to undesired occurrences of inhomogeneous lithium metal deposits, while single lithium-ion conducting (SLIC) polymer electrolytes could mitigate localized ion depletion at electrolyte|electrode interfaces.[8–10] In cases where the anion is immobilized at the polymer side-chains or directly at the polymer backbone, merely Li^+ are mobile thereby enabling t_{Li+} values of 0.9 up to unity.[11,12] Though these materials have demonstrated superior properties regarding lithium ion flux or lithium metal deposition, as well as reasonable limiting current densities, according to recent reports, their mechanical stiffness often requires the presence of plasticizers and/or blending partner(s) to maintain these desirable properties.[11,13–17] Upon incorporation of plasticizers, the corresponding Li^+ conductivity can be boosted to up to 10^{-3} S cm^{-1} even at room temperature,[16,18,19] while for solid systems, Li^+ conductivites in the range of 10^{-7} to 10^{-5} S cm^{-1} are typically stated.[11,20,21] Plasticizers such as ethylene carbonate (EC), propylene carbonate (PC), dimethyl carbonate (DMC) and flowable oligomers can be regarded as so-called transporter molecules that provide major contributions to the overall achievable charge carrier flux whereas the polymer chains often have minor impact on the observable ion transport. While

their long-term stability and robust cycling are often demonstrated for mid-voltage $LiFePO_4$ cathodes (**Table 1**), their compatibility with high voltage materials such as $LiNi_{0.x}Co_{0.y}Mn_{0.z}O_2$ (NMCxyz) for high energy density cells is investigated less common.

Table 1: Solvent uptake and electrochemical properties of various SLIC polymers.

Material	Plasticizer / Solvent uptake [%]	Ionic conductivity [mS cm^{-1}] / Temp [°C]	Cathode material / Mass loading [mg cm^{-2}]	Initial capacity [mAh g^{-1}] / C-Rate / Capacity retention [%] / cycle number / Temp. [°C]	Ref.
PAES-2/PVdF-HFP	EC:DMC / 110	0.5 / 40	NMC532 / 1.9	149 / 0.5 / 94 / 800 / 40	This work
Li-PBPE/PVdF-HFP	EC:DMC / 116	0.5 / 70	LFP / 0.9	110 / 1 / 95 / 800 / r.t.	[22]
LiPPFE/LAGP/PVdF-HFP	EC:DMC / 91	0.8 / 30	LFP / 1.9-2.1	138 / 1 / 95 / 800 / 25	[23]
LiPHFE/PVdF-HFP	EC:DMC / ≈125	0.4 / 25	LFP / 3-5	≈105 / 1 / 95 / 800 / r.t.	[24]
LiPSI/PVDF-HFP	EC:DMC / 145	0.7 / 25	-	110 / 1 / 90 / 1000 / r.t.	[17]
EVOH-graft-LICPSI/PVdF-HFP	EC:DMC / 122	0.1 / 80	LFP / 0.8*	100 / 1 / 95 / 500 / r.t.	[25]
PSiO/PVdF-HFP	EC:DEC:FEC / 130	0.8 / 40	NMC622 / 2.3	148 / 1 / 87 / 500 / 40	[26]
6FPSF-FPES	EC / 240	0.7 / 40	NMC811 / 2.3	≈140 / 1 / 95 / 160 / 40	[27]
SI10-05	PC / 240	1 / 40	NMC811 / 2.0	≈160 / 0.5 / 80 / 443 / 20	[14]

*active material mass loading

In addition, poly(vinylidene fluoride-co-hexafluoropropylene) (PVdF-HFP) is often reported as blending partner or as matrix polymer to both improve the flexibility and stability of electrolyte membranes and to yield mechanically "free-standing" membranes.[13,16–18,28–31] During the membrane casting, domains may be formed with variable contents of SLIC polymer or PVdF-HFP, among which the plasticizer may not necessarily be evenly distributed.[32] Indeed, PVdF-HFP is known for up-take of considerable amounts of plasticizers,[33,34] which might reduce the availability of transporter molecules within the Li^+ containing phase of the polymer blends. Previously, we introduced a SLIC fluorinated poly (aryleneether-sulfonimide)

homopolymer (PAES-1) synthesized *via* polycondensation of two different aromatic monomers which are linked through an ether bond.[35] This polymer, when blended with PVdF-HFP and soaked with EC:DMC, demonstrated very good Li plating/stripping behavior and stability against Li protrusion as well as excellent cycling stability stability in LFP||Li cells. However, the experimentally achieved ionic conductivity was much lower than theoretically expected from atomistic molecular dynamic (MD) simulations. Upon close inspection, it appeared that domain formation and insufficient flexibility of rigid aromatic polymer backbones most likely limited the fraction of plasticizers within the Li^+ conducting phase.

Here, we demonstrate that tailoring polymer backbones of single-ion conducting electrolytes with respect to better flexibility considerably improves the electrochemical properties of resulting polymer blend membranes. By replacing stiff ether linkers between the two aromatic monomers with more flexible -OCH_2CH_2O- moieties (**Figure 1,** PAES-2), the glass transition of the polymers is considerably decreased, and beneficial effects of chemical modification on materials properties such as the ionic conductivity after swelling with EC:DMC and EC:PC mixtures are explored. Notably, much higher limiting current densities are achieved for polymer electrolytes with -OCH_2CH_2O- linker, demonstrating enhanced Li^+ transport. Based on MD simulations, these observations are attributed to the high availability of transporter molecules within the Li^+ conducting phase. Impressive electrochemical performance of the introduced polymer electrolyte is demonstrated for NMC532||Li metal cells, thereby affording a noteworthy capacity retention after 800 cycles at moderate rates of 0.5C.

2. EXPERIMENTAL

2.1 MATERIALS

4-fluorobenzenesulfonyl chloride (97%) and 4-fluorobenzenesulfonamide (97%) were purchased from *Fluorochem Ltd.* and *Apollo Scientific*. 2,2-bis(4-hydroxyphenyl)-

hexafluoropropane (98%) was received from *TCI* and recrystallized from toluene before usage. Sodium hydride (90%), triethylamine (99%), sodium carbonate (99.5%), sodium hydroxide (98%) and lithium bis(trimethylsilyl)amide (1M in tetrahydrofuran), tetrahydrofuran (anhydrous, 99.9%), N,N-dimethylacetamid (DMAc, anhydrous, 99.5%), 1-methyl-2-pyrrolidinone (anhydrous, 99.5%), acetonitrile (99%), dichloromethane (99.8%) and dimethyl sulfoxide (99%) were bought from *Sigma Aldrich/Merck* and used as received. N-hexane (95%, HPLC grade) and diethyl ether (99%) were purchased from *Thermo Fisher Scientific*, dried by an in-house solvent purification system and stored over molecular sieves. Hydrochlorid acid (37% in water, fuming) was purchased from *VWR*. The polymers PVdF-HFP and PVdF were received from *Arkema* and EC, PC as well as DMC (battery grade) were ordered from *BASF Germany*. Cathode active materials NMC622-PCr (polycrystalline) and NMC532-SCr (single crystalline) were purchased from *BASF* and *CATL*, respectively. Super P was received from *Timcal* and lithium metal (500 µm) was taken from *China Energy Lithium Co., Ltd*, which was roll-pressed to a thickness of 300 µm prior to usage.

2.2 SYNTHESIS

2.2.1 Synthesis of Sodium Bis((4-fluorophenyl)sulfonyl)imide (FPSI)

Sodium bis((4-fluorophenyl)sulfonyl)imide (FPSI) was synthesized *via* the Hinsberg reaction as described elsewhere.[35] Thus, 4-fluorobenzenesulfonyl chloride (30.00 g, 154.2 mmol) and 4-fluorobenzenesulfonamide (27.01 g, 1 equiv.) were dissolved in dry acetonitrile (102 mL) in a 500 mL schlenk flask under argon atmosphere. The solution was cooled to 0 °C followed by quick addition of triethylamine (50.9 mL, 2.37 equiv.). After stirring the solution for 12 hours at room temperature, the solvent was removed *via* rotary evaporation. To the resulting brownish oil, an aliquot of 30 mL deionized water was added and the mixture was slowly poured into an aqueous solution of sodium hydroxide (2 M, 600 mL). Thereby, the crude product precipitated,

was filtered off and washed with dichloromethane twice. To purify the product and remove residual sodium hydroxide, the filtered residue was slowly dissolved in acetone, filtrated and collected as fine white powder by titration from dichloromethane (yield: 39.43 g, 72%). (NMR spectra: **Figure S1**)

^{1}H NMR (400 MHz, DMSO-d6) δ [ppm]: 7.67 (d, 4H, Ar-H), 7.18 (d, 4H, Ar-H). **^{13}C{H} NMR (101 MHz, DMSO-d6) δ [ppm]:** 162.88 (d), 142.56 (d), 128.88 (d), 114.76 (d). **^{19}F{H} NMR (376 MHz, DMSO-d6) δ [ppm]:** -110.87 (s).

2.2.2 Synthesis of 2,2-Bis(4-(β-hydroxyethoxy)phenyl)hexafluoropropane (HEPFP)

Synthesis of 2,2-bis(4-(β-hydroxyethoxy)phenyl)hexafluoropropane (HEPFP) was adapted from reported procedures.[36] 2,2-bis(4-hydroxyphenyl)hexafluoropropane (6F-BPA, 31.66 g, 94.17 mmol) was added to EC (16.56 g, 2 equiv.) within a schlenk flask under argon atmopshere at elevated temperatures (>40 °C). Then, sodium carbonate (0.11 g, 0.01 equiv.) was added as catalyst, a condenser attached to the flask and the solution heated up to 170 °C. The mixture was left stirring for 48 hours before being cooled down. Afterwards, the oil was slowly dissolved in dichloromethane (400 mL). The organic phase was washed with aqueous sodium hydroxide (0.1 M, 200 mL) three times, dried over magnesium sulfate and solvents were removed *via* rotary evaporation. The final product (32.37 g, 81%) was obtained as sticky, viscous oil after further drying at 90 °C under reduced pressure (10^{-3} mbar). (NMR spectra: **Figure S2**)

^{1}H NMR (400 MHz, DMSO-d6) δ [ppm]: 7.23 (d, 4H, Ar-H), 7.03 (d, 4H, Ar-H), 4.91 (t, 2H, -COH), 4.02 (t, 4H, -CH_2), 3.72 (m, 4H, -CH_2). **^{13}C{H} NMR (101 MHz, DMSO-d6) δ [ppm]:** 159.4 (s), 131.3 (s), 124.5 (m), 124.4 (s), 114.8 (s), 69.9 (s), 63.3 (m), 59.8 (s). **^{19}F{H} NMR (376 MHz, DMSO-d6) δ [ppm]:** -63.57 (-CF_3).

2.2.3 Polycondensation

Polycondensation was performed by dissolving HEPFP (1.07 g, 2.53 mmol) in 25 mL DMAc under argon atmosphere, then sodium hydride (0.16 g, 2.4 equiv.) was added and the solution was left stirring for two hours. Subsequently, FPSI (0.90 g, 2.53 mmol) was added and the solution heated up to 80 °C under strong stirring. After 48 hours, the reaction was stopped by cooling down the solution to room temperature, filtering it and pouring the filtrate into aqueous hydrochloric acid (1M, 500 mL). The precipitated polymer was collected *via* filtration, washed with water and dried under reduced pressure (10^{-3} mbar). To remove oligomers, dialysis was done with dimethyl sulfoxide : water (3:1) mixture as solvent. The solvent was changed once after 48 hours and the dialysis continued for 72 hours. Afterwards, the polymer was precipitated by addition of aqueous hydrochloric acid, followed by subsequent filtration and drying of the polymer powder (yield: 0.91 g, 50%) at 90 °C under reduced pressure (10^{-3} mbar). (NMR spectra: **Figure S3**)

^{1}H NMR (400 MHz, DMSO-d6) δ [ppm]: 7.59 (4H, Ar-H), 7.24 (4H, Ar-H), 7.09 (4H, Ar-H), 6.99 (4H, Ar-H), 4.37 (s, 8H, -CH_2). **^{19}F{H} NMR (400 MHz, DMSO-d6) δ [ppm]:** -63.55 (-CF_3).

2.2.4 Lithiation of PAES-2

The polymer from the previous step was dissolved in tetrahydrofurane and the solution cooled down to – 40 °C, then lithium bis(trimethylsilyl)amid was added dropwise. After complete addition of the lithium base, the reaction was allowed to heat up to room temperature and stirred for additional 12 hours. Then, solvent was removed *in vacuo*, dry hexane added and the solution vigorously stirred for one day. Afterwards, the polymer was filtered off, washed with a small amount hexane and diethylether, then dried at 90 °C under reduced pressure (10^{-3} mbar) yielding 0.88 g (96%). (NMR spectra: **Figure S4**)

^{1}H NMR (400 MHz, DMSO-d6) δ [ppm]: 7.57 (4H, Ar-H), 7.25 (4H, Ar-H), 7.10 (4H, Ar-H), 6.94 (4H, Ar-H), 4.36 (s, 8H, -CH_2). **^{7}Li NMR (400 MHz, DMSO-d6) δ [ppm]:** -1.02. **^{19}F{H} NMR (400 MHz, DMSO-d6) δ [ppm]:** -63.55 (-CF_3).

2.2.5 Synthesis and Lithiation of PAES-1

PAES-1 was prepared by polycondensation of FPSI with 6F-BPA followed by lithiation according to a previously reported procedure.[35] (NMR spectra: **Figure S5**)

^{1}H NMR (400 MHz, DMSO-d6) δ [ppm]: 7.71 (4H, Ar-H), 7.39 (4H, Ar-H), 7.11 (8H, Ar-H). **^{19}F{H} NMR (400 MHz, DMSO-d6) δ [ppm]:** -63.42 (-CF_3).

2.3 MEMBRANE PREPARATION

PVdF-HFP was dissolved in 6 mL DMAc, then PAES-1 or PAES-2 was slowly added to the solution under stirring (ratio of PVdF-HFP:PAES 1:3). The suspension was cast into a polytetrafluoroethylene dish and dried at 80 °C for 24 hours. To remove residual solvents inside the polymer membranes, they were dried under reduced pressure (10^{-3} mbar) at 80 °C for another 24 hours. Finally, the membranes were swollen with an EC:PC or EC:DMC mixture (1:1 v/v), resulting in overall membrane thicknesses of ≈ 80-90 µm. The solvent uptake was calculated based on the equation

$$SU = \frac{w_s - w_0}{w_0} \cdot 100\% \qquad (1)$$

with w_s and w_0 denoting the weight of the swollen and dry membranes, respectively. Before measuring the solvent uptake, the membranes were carefully dabbed with a tissue to remove droplets on the surface of the membrane.

2.4 CATHODE PREPARATION

Electrodes were prepared by wet casting of electrode paste containing 90 wt.-% active material (NMC532-SCr as received and NMC622-PCr with a 0.5 wt.-% $LiNbO_3$-coating as reported previously[37]), 7 wt.-% conductive agent (carbon black, Super C65), and 3 wt.-% PVdF. First, PVdF was dissolved in 1-methyl-2-pyrrolidinone, then the other components were added and mixed with a *Thinky* planetary mixer at 1500 rpm for 20 minutes. The electrode paste was cast onto aluminum foil (20 µm) using a doctor blade (*Zeiss*) set to a wet-film thickness of 50 µm, dried at 80 °C and were then calendered to a porosity of 30%. The average mass-loading of the electrodes was 2.1 mg cm^{-2} for the NMC622 electrodes and 1.9 mg cm^{-2} for the NMC532 electrodes. To further enhance contacts between cathode particles and the polymer, the electrodes were spin-coated using 30 µL of PAES-2 solution (10 wt.-% in DMAc). The solution was added dropwise onto electrode disks while increasing rotation speed stepwise to 120 rps and holding it for 120 seconds. Finally, the electrodes were dried again to remove residual DMAc.

2.5 MATERIAL CHARACTERIZATION

2.5.1 Gel Permeation Chromatography

Measurement of the molecular weight from polymers was done with an Agilent 1260 Infinity (*Agilent Technologies*) instrument equipped with PolyPore columns and a differential refractive index (RI) detector. DMAc containing 0.03 wt.-% lithium bromide was utilized at 50 °C with a flow rate of 1 mL min^{-1}; the gel permeation chromatography (GPC) system was calibrated using linear poly(methyl methacrylate) standards ranging from 800 to $2.2 \cdot 10^6$ g mol^{-1}. Typically, 100 µL of a 1.0 mg mL^{-1} sample solution was injected onto the columns.

2.5.2 Thermogravimetric Analysis / Differential Scanning Calorimetry

For measuring differential scanning calometry (DSC), a DSC2500 under nitrogen from *TA Instruments* was used with a heating rate of 10 K min^{-1} between -75 to 325 °C (2 ramps). Thermogravimetric analysis (TGA) was conducted on a TGA5500 from *TA Instruments* under helium with a heating rate of 10 K min^{-1}.

2.5.3 Scanning Electron Miscroscopy

Scanning electron microscopy (SEM) investigations were performed at a *Carl Zeiss* AURIGA CrossBeam workstation with a Schottky field emission gun. Images were obtained with a secondary electron detector at an acceleration voltage of 3 kV and a working distance of 3 mm.

2.6 ATOMISTIC MOLECULAR DYNAMICS SIMULATIONS

Atomistic molecular dynamics (MD) simulations were performed using Atomistic Polarizable Potentials for Liquid, Electrolytes, and Polymers (APPLE&P) force fields developed by *Wasatch Molecular Incorporated* (WMI-MD).[38–40] It was shown in previous investigations, that the considered force fields accurately predict the behavior of solid polymer electrolytes.[41–43] A Nosé−Hoover thermostat (frequency of 0.01 fs^{-1}) and Anderson−Hoover barostat (frequency of 0.0005 fs^{-1}) were exploited to control both temperature and pressure of the system.[44,45] Each atomic center was assigned isotropic polarizability and to avoid polarization catastrophe at short distances, a Thole screening parameter of 0.2 was used. With the SHAKE algorithm (tolerance of 10^{-14}) all chemical bonds were constrained.[46] For a cost-efficient simulation, a multiple time-step integration scheme was incorporated.[47,48] Three time steps were chosen: 0.5 fs for bonds, bends and improper torsional motions, 1.5 fs for dihedrals and short-range (< 8.0 Å) nonbonded interactions, and 3 fs for all other nonbonded interactions. A 3 fs time step was also employed for the reciprocal part of the Ewald summation. With the

Ewald summation technique the electrostatic interactions were computed (cutoff: 15 Å; inverse Gaussian charge width: 0.23 $Å^{-1}$; k-vectors: 7 x 7 x 7).[49] The same cutoff of 15 Å was used for van der Waals interactions.

2.7 ELECTROCHEMICAL MEASUREMENTS

Ionic conductivities were derived based on electrochemical impedance spectroscopy (EIS) with an Autolab PGStat302 N potentiostat equipped with the frequency analyzer FRA32 (*Deutsche Metrohm GmbH & Co. KG*) at temperatures ranging from 0 to 70 °C (10 °C steps) and in a frequency range of 1 MHz – 1 Hz, applying a voltage amplitude of 10 mV. A polymer membrane of known dimensions was placed between two polished stainless-steel electrodes in coin cells. The cells were initially heated to 70 °C to improve interfacial contacts between electrodes and electrolyte. Limiting current density, t_{Li}^{+} and Li plating experiments were conducted on VMP3 multichannel potentiostats (*Bio-Logic Science Instruments*) by sandwiching the polymer membrane between two Li metal disks in coin cells with symmetric (two) electrode configuration. Determination of the limiting current density was conducted by increasing the current density at steps of 1 μA s^{-1} at 40 °C until a cut-off voltage of 5 V was reached or the cells were shorted. The t_{Li}^{+} was measured by applying the method proposed by Evans *et al*.[50]; prior to and after applying a polarization voltage ΔV of 10 mV, the impedance of the cells was measured and t_{Li}^{+} derived according to the expression

$$t_{Li}^{+} = \frac{I_{ss}(\Delta V - I_0 R_0)}{I_0(\Delta V - I_{ss} R_{ss})} \qquad (2)$$

where I_0 and I_{ss} denote the initial and steady state current, while R_0 and R_{ss} are the initial and steady state resistances of the interface. The electrochemical stability window was measured in a three-electrode configuration (*Swagelok*)[51] using copper or platinum as working electrodes and lithium metal as both counter and reference electrodes at a scan rate of 0.1 mV s^{-1}. Cycling

investigations were performed with a LBT20084 battery cycler (*Arbin Instruments*) in the voltage range of 3.0 to 4.3 V at 40 °C. Long-term cycling starts with the formation procedure, consisting of cell charge/discharge at slow rates of $2 \cdot 0.05$C and $2 \cdot 0.1$C, respectively, followed by stepwise increase of rates from 0.05C to 0.5C (assuming a theoretical specific capacity of 180 mAh g^{-1} for NMC532-SCr / NMC622-PCr).

3. RESULTS AND DISCUSSION

3.1 SYNTHESIS AND POLYMER CHARACTERIZATION

To increase the flexibility of the highly aromatic PAES-1, the ether moiety -OCH_2CH_2O- was incorporated as bridging group into the polymer backbone by reaction of 6F-BPA with EC (**Figure 1**).[36] A successful condensation polymerization is demonstrated by disappearence of ^{19}F NMR signals from FPHSI at -110.87 ppm and the merging of the two ^{1}H signals at 4.02 ppm and 3.72 ppm from the -CH_2- groups in the ether chain due to similar chemical environments after polymerization (**Figure S3**).

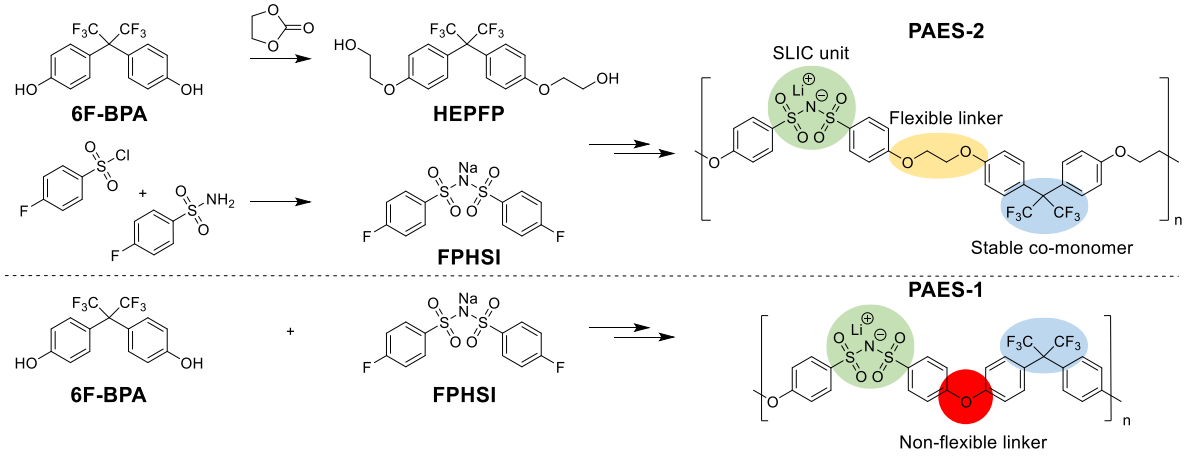

Figure 1: Synthesis scheme for PAES-1/PAES-2 and structural comparison of both polymers. The non-flexible linker of PAES-1 (red) is exchanged by a more flexible ethylene glycol entity (yellow).

Deprotonation of an aliphatic alcohol requires strong bases such as sodium hydride, thereby limiting the accessible reaction temperature for the condensation polymerization, thus resulting in lower molecular weights of PAES-2 compared to PAES-1. For better comparability, the smaller oligomers were removed by dialysis, yielding an increase of the molecular weight from 14.9 kDa to 30.6 kDa and a more uniform weight distribution (**Figure 2a**). Though the existing difference in polymer molecular weights of PAES-1 and PAES-2 (M_N of 65 kDa[35] *vs.* 30.6 kDa) may have an effect on the corresponding polymer and membrane properties, it is assumed that the impact is much smaller than that from modifying the chemical structure. The glass transition temperature, T_g, was measured to get insights into the polymer chain mobility. A decrease of T_g of 277 °C for PAES-1 to 147 °C in case of PAES-2 (**Figure 2b**), suggests lower crystallinity of the polymer after modification. The Fory-Flox equation

$$T_g = T_{g,\infty} - \frac{K}{M_n} \qquad (3)$$

describes the dependence between T_g and M_N with $T_{g,\infty}$ being the glass transition temperature at theoretical infinite molecular weight and K being an empirical parameter related to a "free volume" in the polymer sample.[52,53] Note that T_g can change distinctly at low M_N values, but often rises quickly towards a plateau value with higher M_N.[54,55] Therefore, it can be assumed that the measured difference in T_g between PAES-1 and PAES-2 is mainly caused by modification of the chemical structure and not due to differences in the molecular weight. The thermal stability is also affected by the structural modification as PAES-2 decomposition that starts at an onset temperature of 360 °C, thus earlier than in case of PAES-1, reflecting the presence of linear ether chains in the polymer backbone (**Figure 2c**). Nevertheless, the threshold for thermal decomposition remains sufficiently high to permit its application as quasi-solid electrolytes in lithium metal batteries.

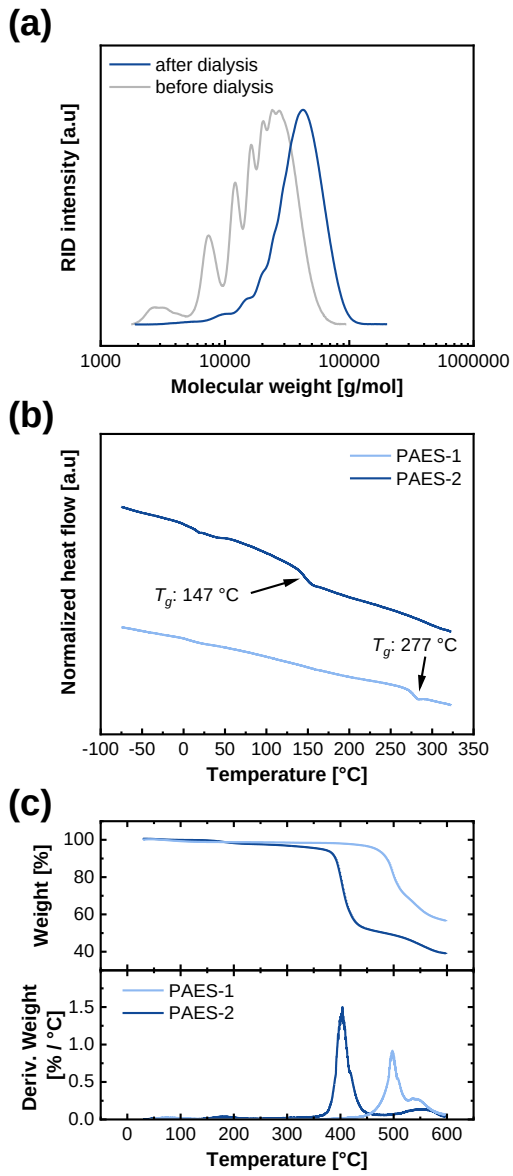

Figure 2: (a) Molecular weight distribution of PAES-2 before and after dialysis in DMSO:H_2O, measured *via* gel permeation chromatography, (b) DSC thermograms of the second heating ramp for PAES-1 and PAES-2 and (c) the corresponding TGA curves.

3.2 IONIC CONDUCTIVITY

PAES-2, with its high glass transition temperature, requires blending with a flexible polymer such as PVdF-HFP to form stable, self-standing membranes. In analogy to other reported SLIC polymers, a weight ratio of 3:1 was established as a good compromise between achieving membrane stability and maintaining high ionic conductivity, as further increasing the PVdF-

HFP content would lead to a decrease of ionic conductivity due to the absence of Li^+ in the PVdF-HFP phase.[13,35] The membranes obtained *via* solvent-casting have an average thickness of 80-90 µm (**Figure 3a,b**) and are denoted as PAES-1b and PAES-2b. After immersing the membranes for at least 48 hours in EC:DMC (1:1 v/v) and EC:PC (1:1 v/v), flexible membranes were obtained that simultaneously retain the solvent inside the polymer matrix.

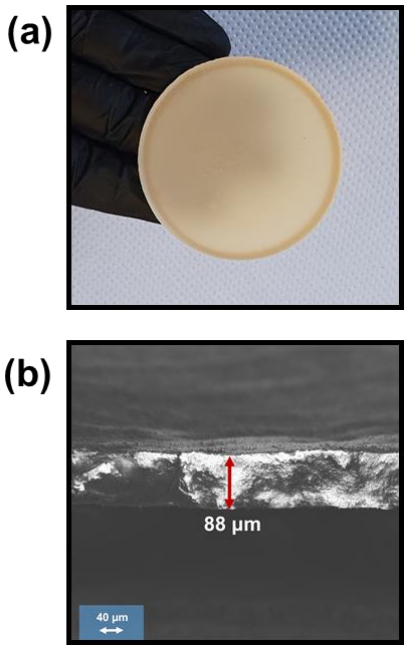

Figure 3: (a) Image of the dry polymer membrane after solvent casting and (b) SEM cross-section of the polymer membrane.

The determined ionic conductivities of PAES-2b in the temperature range of 0–70 °C are higher than the data obtained for PAES-1b in case of both solvent mixtures (**Figure 4a**). In combination with EC:DMC, the maximum conductivity of PAES-2b reaches 0.73 mS cm^{-1} at 70 °C, whereas merely 0.11 mS cm^{-1} is achieved for the corresponding PAES-1b membranes, demonstrating enhanced ion transport properties within PAES-2b membranes. At temperatures ≤ 10 °C, the ionic conductivity for membranes swollen in EC:DMC decreases considerably due to crystallization of EC and DMC and, thus, restricted Li^+ transport. The high standard deviation at 10 °C arises from differences in impedance between cooling and heating runs, as residual

electrolyte may remain crystallized at this temperature step during the heating run. The absence of this effect in membranes containing PC is attributed to its lower melting point, highlighting suitability of solvent combinations of EC:PC at low temperatures. Clearly, the plasticizer combination EC:DMC yields higher overall ionic conductivities compared to EC:PC (*e.g.*, 0.51±0.16 mS cm^{-1} *vs.* 0.33±0.07 mS cm^{-1} @ 40 °C), consistent with a slightly higher solvent uptake and a lower viscosity of this plasticizer (**Figure 4b**).[56] However, the high vapor pressure of DMC induces its evaporation, as demonstrated by the TGA curves in **Figure 4c**, even when mixed with EC. This can lead to EC crystallization at the membrane's surface if the membrane is exposed to unsealed environments for a prolonged duration (**Figure S7**). As this phenomenon might occur in other gel polymer electrolytes, it is strongly advised to carefully handle polymer membranes when utilizing plasticizers such as EC:DMC. The Li^+ concentration in the PAES-2b membrane is estimated to be approximately 1.4 mol/L, based on the weight of the dry membrane and the dimensions of the swollen membrane. A comparison with a liquid electrolyte of similar concentration, 1.4M LiTFSI in EC:PC or EC:DMC (1:1 v/v), soaked in a PVdF-HFP membrane (**Figure S8**), shows that the ionic conductivities are of a similar magnitude. Therefore, the use of the PAES-2b polymer as a Li^+ source, instead of a traditional lithium salt, does not negatively affect the ionic conductivity.

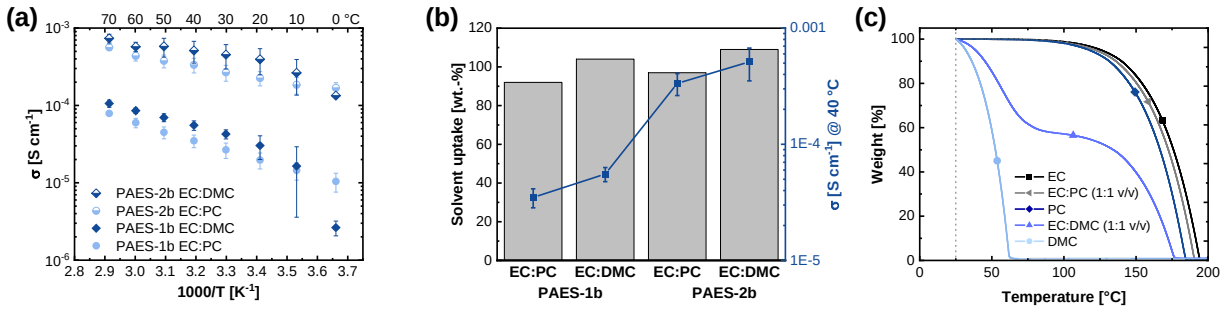

Figure 4: (a) Ionic conductivity of PAES-1b and PAES-2b membranes with EC:PC and EC:DMC as solvent in a temperature range from 0 °C to 70 °C (combined heating and cooling

runs), (b) solvent uptake of electrolyte membranes and their respective ionic conductivities at 40 °C and (c) TGA measurements of different solvent mixtures.

3.6 MEMBRANE MORPHOLOGY AND POLYMER ARRANGEMENT

Besides solvent uptake of the polymer membrane, morphology, polymer arrangement and solvent distribution within the polymer blend membrane impact Li^+ transport properties. The PAES-2b membrane has micropores in the range 1 – 5 µm while for PAES-1b only nanometer sized pores are visible in SEM images (**Figure 5a,b**), elucidating the slightly higher solvent uptake shown in **Figure 4b**. It should be noted that according to literature, blending of aromatic polymers with PVdF-HFP often results in a formation of pores[29,57–59] while aliphatic polymers tend to yield denser structures.[25,60,61] However, functional groups at the backbone can greatly affect the porosity by changing the miscibility with the PVdF-HFP blend partner despite being highly aromatic.[41] Notably, to unravel Li^+ coordination, actual solvent distribution and polymer arrangement within the blend membranes, atomistic MD simulations of the two polymers with overall solvent uptakes of 70 and 140% EC:DMC and EC:PC were performed. A snapshot of such a simulated box is displayed in **Figure 5c**, with further details regarding aspects of the structure, number and molecular weight of polymer constituents as well as the total number of plasticizer molecules listed in the appendix. Through analysis of the radial distribution function (RDF), information regarding the general coordination and the composition of the first Li^+ coordination shell can be obtained. The main contributors to Li^+ interaction and coordination are atoms with negative partial charges, including double bounded O atoms in EC, PC, DMC and the $-S(O)_2N^-S(O)_2-$ group of the SLIC polymer, as exemplified in **Figure 5d** for a system containing 140% EC:DMC. From the SLIC polymer, only the oxygen of the anionic group contributes to the coordination while the negatively charged nitrogen atoms and the ether oxygens of the $-OCH_2CH_2O-$ linker are not participating. The coordination numbers within a 2.7 Å radius (first minimum after defined peaks in RDF plots) around Li^+ are examined to

determine the composition of the first coordination shell for Li^+. Regardless of solvent composition (EC:PC or EC:DMC) and content (70% and 140%), the total coordination number amounts to ≈ 4, similar to bulk solutions of EC with LiTFSI,[62] from which the major contributor is O_{anion} followed by $O_{solvent}$ (**Figure 5e**). An increase of solvent molecules within the simulated box results in slightly higher coordination numbers as more $O_{solvent}$ atoms can interact with Li^+ while the amount of O_{anion} atoms of the polymer group remain constant.

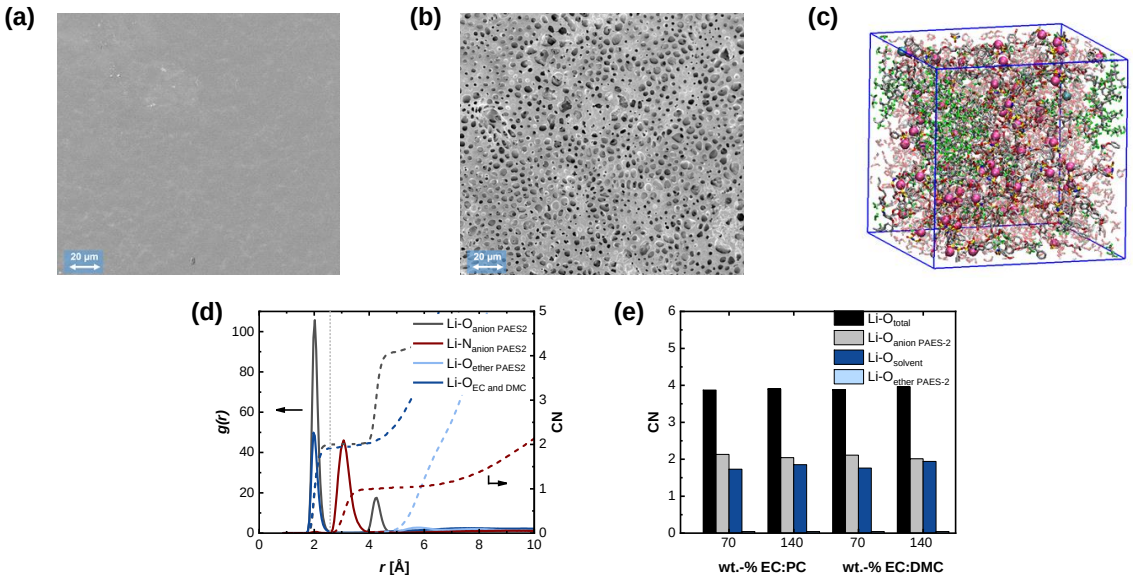

Figure 5: SEM images of a dry (a) PAES-1b membrane and (b) PAES-2b membrane; (c) snapshot of box applied in MD simulations containing PAES-2, PVdF-HFP, Li^+ and solvent (EC:DMC or EC:PC mixture), (d) Li^+-O RDFs (solid line) and coordination number (dashed line) of PAES-2b with 140 wt.-% EC:DMC, (e) comparison of the coordination numbers of PAES-2b systems with different solvent compositions and contents.

Besides Li^+ coordination, the overall distribution of PAES-2 and PVdF-HFP within the box can be analyzed too see whether the polymers are homogeneously mixed or if certain species accumulates. Hence, the RDFs of $O_{ether,PAES-2}$-$O_{ether,PAES-2}$ representing PAES-2 and $F_{Polymer}$-$F_{Polymer}$ representing PVdF-HFP are compared (**Figure 6a**). Atoms from the same and separate molecules are differentiated from each other with the solid line representing inter- and

intramolecular atoms while the dotted line only represents intermolecular atoms. For inter- and intramolecular atoms both RDFs show high peaks at well-defined distances due to spatial proximity of functional groups within the same polymer chain. However, if only intermolecular atoms are taken into consideration, the RDF of $O_{ether,PAES-2}$-$O_{ether,PAES-2}$ is ≈1, indicating random distribution of PAES-2 within in the box. A RDF >1 for $F_{Polymer}$-$F_{Polymer}$ suggests the occurrence of aggregation and formation of PVdF-HFP rich domains. These results can also be observed in snapshots from the simulated box (**Figure 6b**), where PAES-2 seems to be randomly distributed and PVdF-HFP aggregates at certain spots. In order to obtain information regarding the solvent distribution within these polymer structures, the RDFs between the center of masses of the polymers (C_{SLIC} / $C_{PVdF-HFP}$) and the solvent molecules (C_{EC}, C_{PC}, C_{DMC}) are analyzed (**Figure 6c**). The solvent molecules are randomly distributed around PAES-2 (RDF value of ≈ 1), but are less present around PVdF-HFP (RDF value of << 1). Note that in previous work regarding blend membranes of polymer PAES-1 and PVdF-HFP, an accumulation of solvent molecules within the PVdF-HFP was assumed due to the unfavorable high stiffness of polymer PAES-1.[35] For the newly introduced polymer PAES-2, the opposite effect is observed in the MD simulations, which could explain the experimentally determined higher ionic conductivities of PAES-2b compared to PAES-1b (**Figure 4a**) and highlights the benefits of the more flexible linker in the polymer backbone.

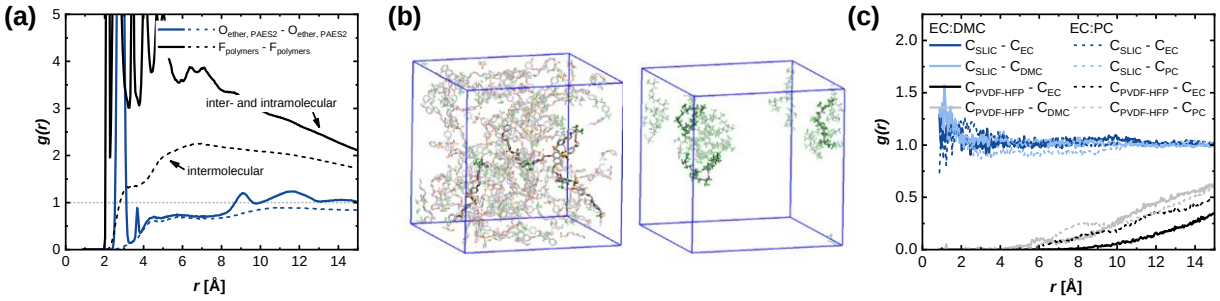

Figure 6: (a) RDF of $O_{ether,PAES-2}$-$O_{ether,PAES-2}$ from PAES-2 and $F_{Polymer}$-$F_{Polymer}$ from PVdF-HFP; the solid line includes inter- and intramolecular atoms while the dashed line only

represents intermolecular atoms, (b) snapshots of the spatial distribution of both polymers inside the box and (c) RDF of the center of masses from polymers to solvent molecules.

3.4 ELECTROCHEMICAL FEATURES OF THE ELECTROLYTE

The critical current density, which was measured by application of a current sweep in symmetric Li||Li cells and simultaneously observation of the voltage response, can also give further insights into Li^+ transport properties of the electrolyte. For PAES-1b, an increase in overvoltage during the current sweep leads to approach of the cut-off threshold of 5 V at current densities of 1.4 and 2.0 mA cm^{-2} for EC:PC and EC:DMC, respectively (**Figure 7a**). Meanwhile, the PAES-2b membranes demonstrates a much slower linear increase of the cell voltage, resulting in cell shorting at impressively high current densities of 3.7 mA cm^{-2} (EC:PC) and 4.0 mA cm^{-2} (EC:DMC) due to Li protrusion. Cell shorting was confirmed by measuring impedance after linear sweep voltammetry (**Figure S10a**). Comparing these results with liquid electrolyte 1M LiTFSI in EC:DMC (1:1 v/v) (**Figure S11a**), cell shorting occurs at almost the same current density (4.3 mA cm^{-2}) even though the applied separator (250 µm) is much thicker than the PAES-2b membrane. The high applicable current densities and low overvoltage indicate very good Li^+ transport within the PAES-2b membranes. It should be noted that for SLIC polymers in contrast to dual-ion conducting polymers no strong concentration polarization is expected since immobilized anions cannot move to the opposite electrode, so that actually no Li^+ depletion occurs.[63] Therefore, a nearly linear voltage increase is observed representing Ohmic response of the system. **Figure S11b** displays linear sweep voltammetry of crosslinked PEO with LiTFSI where upon Li^+ depletion, the observable cell voltage increases exponentially. In the case of PAES-1b a non-linear response is observed, probably due to small amounts of residual other ions (anions), resulting in minor ion depletion and polarization. It should be noted that the measurement results are impacted not only by the membrane properties but also by external factors such as the applied pressure within the cells, which can enhance

contacts to the Li metal electrodes.[64] To confirm the SLIC properties of PAES-2b, the t_{Li+} was measured *via* methods proposed by Evans et al.[50] The current response during polarization, along with the Nyquist plots before and after polarization, is depicted in **Figure 7b** for the membrane containing EC:DMC and in **Figure S9** for the one containing EC:PC. A value of t_{Li+} = 0.92 was calculated for both solvent combinations (EC:DMC and EC:PC), which is slightly lower than the theoretically anticipated value of 1 but is in the range of other reported SLIC polymer electrolytes and corroborates SLIC behavior.[11] In addition, the electrochemical stability window was determined *via* linear sweep voltammetry against copper and platinum working electrodes (**Figure 7c**). An exponential increase in current density starting at potentials of 4.2 V – 4.3 V *vs.* Li|Li$^+$ (inlet of **Figure 7c**) during the anodic scan signals the onset of polymer electrolyte degradation. Even though the oxidative stability of the polymer materials is just inside the operation window of high-voltage cathode materials such as $LiNi_{0.x}Mn_{0.y}Co_{0.z}O_2$ or $LiNi_{0.x}Co_{0.y}Al_{0.z}O_2$, the material could be feasible for this application, especially after forming a cathode electrolyte interphase. The reductive scan reflects electrolyte decomposition of EC, PC and DMC or minor traces of solvent from the casting process at 1.5 V – 0.5 V *vs.* Li|Li$^+$ followed by lithium plating at ≈0 V *vs.* Li|Li$^+$.[27,65] For PAES-2b, the decomposition peak appears to be larger, probably because of the higher solvent uptake of the membrane and, thus, higher electrolyte exposure at the electrode surface.

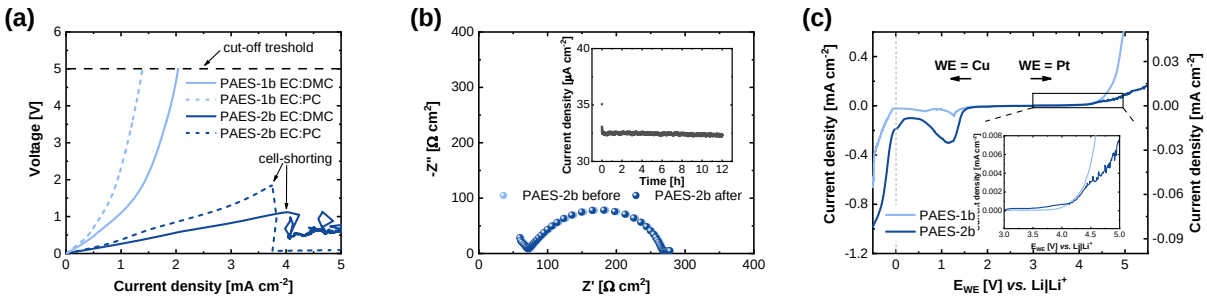

Figure 7: (a) Determination of the critical current density *via* linear sweep amperometry with a scan rate of 1 µA cm^{-2}, (b) Chronoamperometry and Nyquist plots before and after

polarization of a Li||Li cell with PAES-2b membrane, (c) determination of the electrochemical stability window with a scan rate of 0.1 mV s^{-1}.

Long-term stability against Li metal was further investigated by continuous Li plating/stripping (**Figure 8a-b**) at a current density of 0.2 mA cm^{-2} for 1 h (0.2 mAh cm^{-2}). The polymers PAES-1b and PAES-2b with EC:DMC exhibit robust electrochemical cycling performance for hundreds of hours, with overpotentials of 152 mV and 52 mV, respectively, before degradation reactions of the organic carbonates and the polymer, along with changes at the interphases lead to overpotential growth. In case of PAES-2b, the increase in overpotential is less pronounced and starts only after 600 h, demonstrating superior cycling stability. Over the duration of one cycle, the voltage profile of PAES-2b remains flat while for PAES-1b an arching of the overvoltage is monitored. Even during a stepwise increase of the current density, the voltage profile of PAES-2b does not reflect any arching up to 0.66 mA cm^{-2} and results only in minor polarization at 1 mA cm^{-2} (**Figure 8c,d**). Meanwhile, PAES-1b is affected by strong polarization and a rather noisy voltage profile at such current densities, indicating decomposition reactions at the Li metal interface and formation of SEI layers with poor Li^+ transport properties.[66] It should be noted that the limiting current density determined through Li plating/stripping varies considerably from that derived by linear sweep amperometry as higher amounts of Li are stripped/plated back and forth, hence causing larger stress for the polymer membranes.

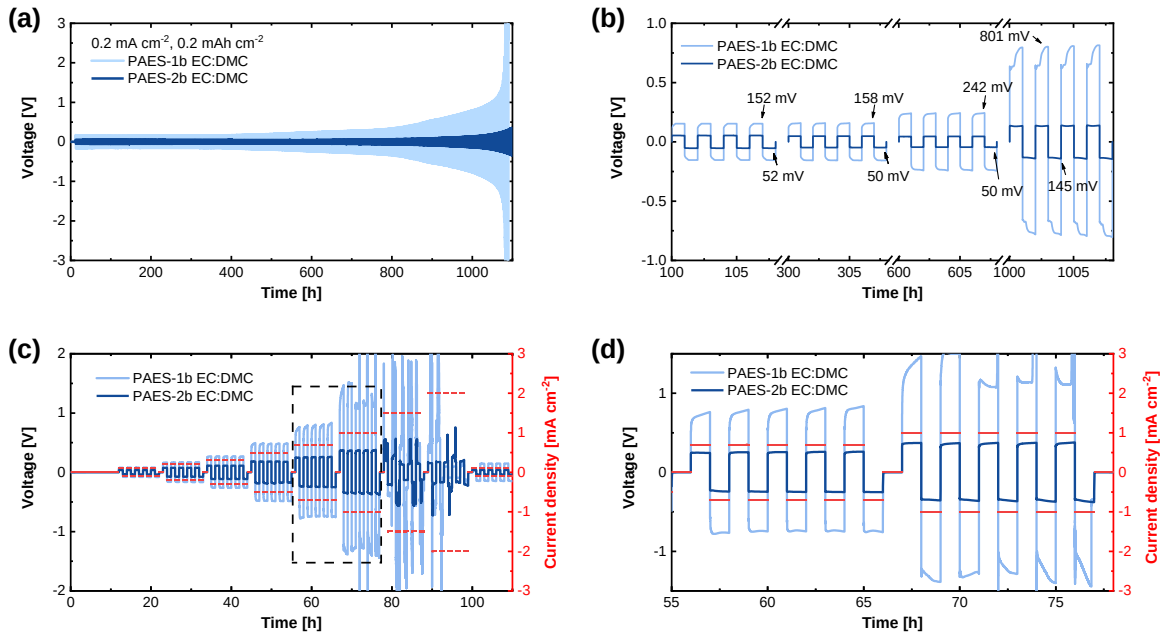

Figure 8: (a) Li plating/stripping of PAES-1b and PAES-2b in Li||Li cells with 0.2 mA cm^{-2} for 1 h (0.2 mAh cm^{-2}) each cycle and (b) voltage profiles of selected cycles during long-term plating/stripping, (c) Li plating/stripping with stepwise increase of the applied current density for 1 h each cycle and (d) zoom into the voltage profiles at current denities of 0.66 mA cm^{-2} and 1 mA cm^{-2} (black inlet).

3.5 CYCLING PERFORMANCE IN NMC||LI CELLS

Among current high-energy-density lithium metal batteries, NMC stands out as a favored cathode material. After replacing the commonly employed poly-crystalline NMC (NMC-PCr) with single-crystalline NMC (NMC-SCr) variants, rather superior electrochemical cycling performance was reported in case of ceramic and polymer electrolytes, attributed to faster Li^+ diffusion within the cathodes.[67–69] Hence, the performance of PAES-2b with both cathode active materials is evaluated in the present work. As the oxidative stability of the polymers was only determined at upper charge potentials between 4.2 – 4.3 V *vs.* Li|Li^+, the NMC622-PCr particles were covered by a $LiNbO_3$-coating[37] while the commercial NMC532-SCr particles are provided

with a Y_2O_3 coating. Prior to cycling, as previously reported, PAES-2 was drop-coated into the cathodes to enhance internal contacts and Li^+ transport properties.[70,71]

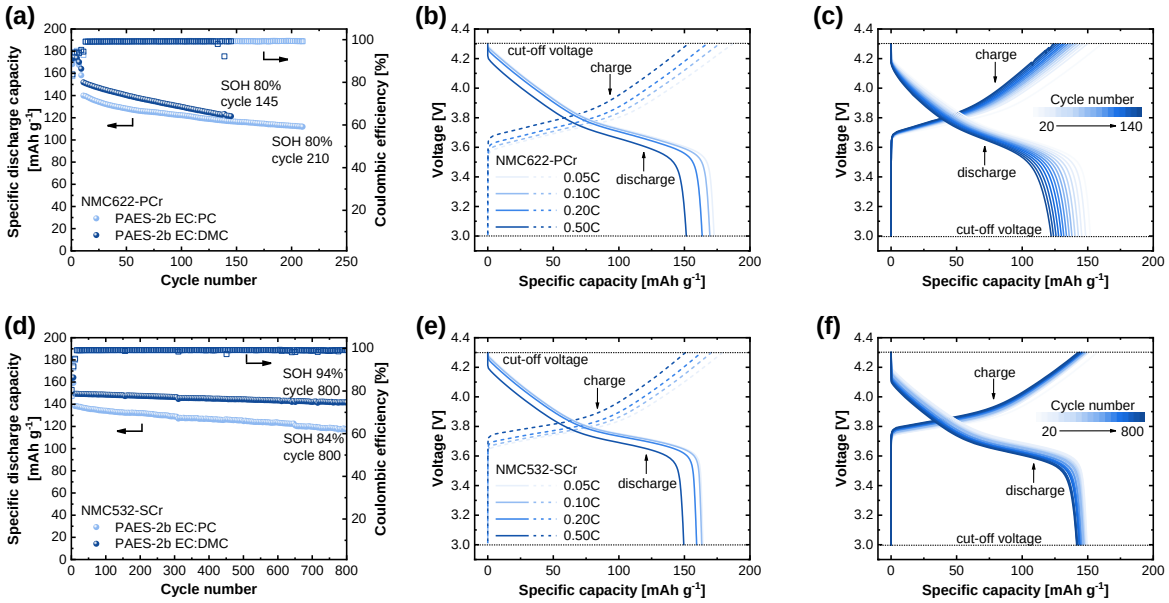

Figure 9: (a) Cycling performance of PAES-2b membranes in NMC622-PCr||Li cells with corresponding (b) voltage profiles at different current densities and (c) voltage profiles of selected cycles (only with EC:DMC); (d) cycling performance of PAES-2b membranes in NMC532-SCr||Li cells with corresponding (e) voltage profiles at different current densities and (f) voltage profile at selected cycles (only with EC:DMC).

In NMC622-PCr||Li cells, the initial discharge capacity for membranes containing EC:DMC is 152.0 mAh g^{-1} at 0.5C (cycle 11), surpassing that of membranes with EC:PC, which yield an initial discharge capacity of ≈140.0 mAh g^{-1} (**Figure 9a**). The higher ionic conductivity of PAES-2b with the plasticizer EC:DMC diminishes polarization phenomena and consequently augments the discharge capacity. PAES-2b with EC:DMC delivers specific discharge capacities of 173 mAh g^{-1} at 0.05C, 169 mAh g^{-1} at 0.1C, 164 mAh g^{-1}at 0.2C and 151 mAh g^{-1} at 0.5C (**Figure 9b**), showcasing adequate capacity retention at higher C-rates. Membranes operated with NMC622-PCr cathodes however suffer from capacity fading upon cycling and a growing voltage hysteresis (**Figure 9c**), resulting in SOH80% after 145 cycles (121 mAh g^{-1}) and 210

cycles (112 mAh g^{-1}) for EC:DMC and EC:PC, respectively. When PAES-2b is being paired with NMC532-SCr cathodes, the cells provide an initial discharge capacity of 149 mAh g^{-1} with EC:DMC and 138 mAh g^{-1} with EC:PC as plasticizer at rates of up to 0.5C (**Figure 9d**). Impressively, the capacity retention remains above SOH80% after more than 800 cycles. Especially, cells containing PAES-2b EC:DMC deliver high capacity retention of 141 mAh g^{-1} (94%) after 800 cycles, with good discharge capacities at various C-rates (**Figure 9e**). Only with robust interphases between the electrolyte membrane and the active materials such high capacity retentions are attained, as evidenced by a minimal increase in voltage hysteresis upon cell operation (**Figure 9f**). It should be noted that the mass loadings of the NMC532-SCr electrodes are marginally lower compared to NMC622-PCr electrodes, which also enhances cycling stability due to lower applied current densities and reduced charge transport during each cycle. Overall, utilizing NMC532-SCr as cathode active material substantially enhances the long-term cycling performance in full cells. To boost electrode mass loadings, novel approaches such as incorporation of oligomers within the cathodes to facilitate higher ion conduction should be considered in the future.

4. CONCLUSION

By systematically tuning the chemical structure of an aromatic SLIC polymer PAES-1, general properties of the blend membranes (with PVdF-HFP) such as the ionic conductivity could be increased 6-fold to 0.5 mS cm^{-1} at 40 °C. The introduced flexible -OCH_2CH_2O- linker (compared to a simple -O- linker) decreases the T_g of the newly synthesized polymer PAES-2 considerably, indicating an improved mobility of the polymer chains. Since the solvent uptake of EC:DMC for PAES-2 and PAES-1 blended with PVdF-HFP increases only slightly (109 *vs.* 104 wt.%), the improved properties suggest a more uniform distribution of solvent molecules in the Li^+ containing phases of the SLIC compared to PVdF-HFP-rich phases. Molecular dynamics simulations are employed to further analyze the Li^+ coordination, the structural

arrangement of PAES-2/PVdF-HFP, and the distribution of solvent within these phases. The results indicate that, upon chemical modification, the solvent prefers the environment of PAES-2b over PVdF-HFP, which favors overall Li^+ transport properties. The designed SLIC polymer electrolytes can be cycled against high-voltage NMC cathodes, where especially in NMC532-SCr||Li cells, high capacity retention of up to 94% after 800 cycles with an initial discharge capacity of 152 mAh g^{-1} at 0.5C is achieved. These results strongly suggests that the chemical structures and domain formation of SLIC polymer electrolytes containing blending partners such as PVdF-HFP and plasticizers need to be designed carefully.

ASSOCIATED CONTENT

Supporting Information

The Supporting Information is available free of charge.

NMR spectra of PAES-1, PAES-2 and polymer precursor; details of molecular dynamics simulation; Image of PAES-2 EC:DMC membrane; Impedance data and Nyquist plots of PAES-1b and PAES-2b; current sweeps of liquid electrolyte formulation and solid polymer PEO

AUTHOR INFORMATION

Corresponding Author

Gunther Brunklaus — Helmholtz Institute Münster, IEK-12, Forschungszentrum Jülich GmbH, 48149 Münster, Germany; E-mail: g.brunklaus@fz-juelich.de

Authors

Gerrit Michael Overhoff — Helmholtz Institute Münster, IEK-12, Forschungszentrum Jülich GmbH, 48149 Münster, Germany

Elisabeth Verweyen — Helmholtz Institute Münster, IEK-12, Forschungszentrum Jülich GmbH, 48149 Münster, Germany

Philipp Roering — Helmholtz Institute Münster, IEK-12, Forschungszentrum Jülich GmbH, 48149 Münster, Germany

Martin Winter — Helmholtz Institute Münster, IEK-12, Forschungszentrum Jülich GmbH, 48149 Münster, Germany; MEET Battery Research Center, Institute of Physical Chemistry, University of Münster, 48149 Münster, Germany

Author Contributions

The manuscript was written through contributions of all authors. All authors have given approval to the final version of the manuscript. G. M. Overhoff: Conceptualization, Investigation, Writing – Original Draft. E. Verweyen: Investigation. P. Roering: Investigation. M. Winter: Writing - Review & Editing, Supervision, Funding Acquisition. G. Brunklaus: Writing - Review & Editing, Supervision, Funding Acquisition.

Notes

The authors declare no competing financial interest.

ACKNOWLEDGMENT

Financial support from the German Federal Ministry of Education and Research (BMBF) within ‘FestBatt’ (FB2-POLY: 13XP0429A; FB2-Hybrid: 13XP0428A) is gratefully acknowledged. The authors thank Dr. Valeriu Mereacre, Dr. Joachim R. Binder and Prof. Helmut Ehrenberg for providing the $LiNbO_3$-coated NMC622-PCr material.

References

(1) Placke, T.; Kloepsch, R.; Dühnen, S.; Winter, M. Lithium Ion, Lithium Metal, and Alternative Rechargeable Battery Technologies: The Odyssey for High Energy Density. *J. Solid State Electrochem.* **2017**, *21* (7), 1939–1964. DOI: 10.1007/s10008-017-3610-7.

(2) Kalhoff, J.; Eshetu, G. G.; Bresser, D.; Passerini, S. Safer Electrolytes for Lithium-Ion Batteries: State of the Art and Perspectives. *ChemSusChem* **2015**, *8* (13), 2154–2175. DOI: 10.1002/cssc.201500284.

(3) Ngai, K. S.; Ramesh, S.; Ramesh, K.; Juan, J. C. A Review of Polymer Electrolytes: Fundamental, Approaches and Applications. *Ionics* **2016**, *22* (8), 1259–1279. DOI: 10.1007/s11581-016-1756-4.

(4) Nair, J. R.; Imholt, L.; Brunklaus, G.; Winter, M. Lithium Metal Polymer Electrolyte Batteries: Opportunities and Challenges. *Electrochem. Soc. Interface* **2019**, *28* (2), 55–61. DOI: 10.1149/2.F05192if.

(5) Lennartz, P.; Paren, B. A.; Herzog-Arbeitman, A.; Chen, X. C.; Johnson, J. A.; Winter, M.; Shao-Horn, Y.; Brunklaus, G. Practical Considerations for Enabling Li|Polymer Electrolyte Batteries. *Joule* **2023**, *7* (7), 1471–1495. DOI: 10.1016/j.joule.2023.06.006.

(6) Xue, Z.; He, D.; Xie, X. Poly(ethylene oxide)-based Electrolytes for Lithium-Ion Batteries. *J. Mater. Chem. A* **2015**, *3* (38), 19218–19253. DOI: 10.1039/C5TA03471J.

(7) Doyle, M.; Fuller, T. F.; Newman, J. The Importance of the Lithium Ion Transference Number in Lithium/Polymer Cells. *Electrochim. Acta* **1994**, *39* (13), 2073–2081. DOI: 10.1016/0013-4686(94)85091-7.

(8) Chazalviel, J.-N. Electrochemical Aspects of the Generation of Ramified Metallic Electrodeposits. *Phys. Rev. A* **1990**, *42* (12), 7355–7367. DOI: 10.1103/PhysRevA.42.7355.

(9) Brissot, C.; Rosso, M.; Chazalviel, J.-N.; Lascaud, S. Dendritic Growth Mechanisms in Lithium/Polymer Cells. *J. Power Sources* **1999**, *81-82*, 925–929. DOI: 10.1016/S0378-7753(98)00242-0.

(10) Tikekar, M. D.; Archer, L. A.; Koch, D. L. Stability Analysis of Electrodeposition across a Structured Electrolyte with Immobilized Anions. *J. Electrochem. Soc.* **2014**, *161* (6), A847-A855. DOI: 10.1149/2.085405jes.

(11) Jeong, K.; Park, S.; Lee, S.-Y. Revisiting Polymeric Single Lithium-Ion Conductors as an Organic Route for All-Solid-State Lithium Ion and Metal Batteries. *J. Mater. Chem. A* **2019**, *7* (5), 1917–1935. DOI: 10.1039/C8TA09056D.

(12) Deng, K.; Zeng, Q.; Wang, D.; Liu, Z.; Qiu, Z.; Zhang, Y.; Xiao, M.; Meng, Y. Single-ion Conducting Gel Polymer Electrolytes: Design, Preparation and Application. *J. Mater. Chem. A* **2020**, *8* (4), 1557–1577. DOI: 10.1039/C9TA11178F.

(13) Borzutzki, K.; Thienenkamp, J.; Diehl, M.; Winter, M.; Brunklaus, G. Fluorinated Polysulfonamide Based Single Ion Conducting Room Temperature Applicable Gel-Type Polymer Electrolytes for Lithium Ion Batteries. *J. Mater. Chem. A* **2019**, *21* (7), 188–201. DOI: 10.1039/c8ta08391f.

(14) Chen, Z.; Steinle, D.; Nguyen, H.-D.; Kim, J.-K.; Mayer, A.; Shi, J.; Paillard, E.; Iojoiu, C.; Passerini, S.; Bresser, D. High-Energy Lithium Batteries based on Single-Ion Conducting Polymer Electrolytes and $Li[Ni_{0.8}Co_{0.1}Mn_{0.1}]O_2$ Cathodes. *Nano Energy* **2020**, *77*, 105129. DOI: 10.1016/j.nanoen.2020.105129.

(15) Cao, C.; Li, Y.; Feng, Y.; Long, P.; An, H.; Qin, C.; Han, J.; Li, S.; Feng, W. A Sulfonimide-based Alternating Copolymer as a Single-ion Polymer Electrolyte for High-

Performance Lithium-ion Batteries. *J. Mater. Chem. A* **2017**, *5* (43), 22519–22526. DOI: 10.1039/C7TA05787C.
(16) Zhong, Y.; Zhong, L.; Wang, S.; Qin, J.; Han, D.; Ren, S.; Xiao, M.; Sun, L.; Meng, Y. Ultrahigh Li-Ion Conductive Single-Ion Polymer Electrolyte Containing Fluorinated Polysulfonamide for Quasi-Solid-State Li-Ion Batteries. *J. Mater. Chem. A* **2019**, *7* (42), 24251–24261. DOI: 10.1039/C9TA08795H.
(17) Li, C.; Qin, B.; Zhang, Y.; Varzi, A.; Passerini, S.; Wang, J.; Dong, J.; Zeng, D.; Liu, Z.; Cheng, H. Single-Ion Conducting Electrolyte Based on Electrospun Nanofibers for High-Performance Lithium Batteries. *Adv. Energy Mater.* **2019**, *8*, 1803422. DOI: 10.1002/aenm.201803422.
(18) Rohan, R.; Sun, Y.; Cai, W.; Zhang, Y.; Pareek, K.; Xu, G.; Cheng, H. Functionalized Polystyrene based Single Ion Conducting Gel Polymer Electrolyte for Lithium Batteries. *Solid State Ion.* **2014**, *268*, 294–299. DOI: 10.1016/j.ssi.2014.10.013.
(19) Oh, H.; Xu, K.; Yoo, H. D.; Kim, D. S.; Chanthad, C.; Yang, G.; Jin, J.; Ayhan, I. A.; Oh, S. M.; Wang, Q. Poly(arylene ether)-Based Single-Ion Conductors for Lithium-Ion Batteries. *Chem. Mater.* **2016**, *28* (1), 188–196. DOI: 10.1021/acs.chemmater.5b03735.
(20) Bouchet, R.; Maria, S.; Meziane, R.; Aboulaich, A.; Lienafa, L.; Bonnet, J.-P.; Phan, T. N. T.; Bertin, D.; Gigmes, D.; Devaux, D.; Denoyel, R.; Armand, M. Single-ion BAB Triblock Copolymers as Highly Efficient Electrolytes for Lithium-Metal Batteries. *Nat. Mater.* **2013**, *12* (5), 452–457. DOI: 10.1038/NMAT3602.
(21) Porcarelli, L.; Shaplov, A. S.; Bella, F.; Nair, J. R.; Mecerreyes, D.; Gerbaldi, C. Single-Ion Conducting Polymer Electrolytes for Lithium Metal Polymer Batteries that Operate at Ambient Temperature. *ACS Energy Lett.* **2016**, *1* (4), 678–682. DOI: 10.1021/acsenergylett.6b00216.
(22) Pan, Q.; Jiang, S.; Li, Z.; Liu, Y.; Du, Y.; Zhao, N.; Zhang, Y.; Liu, J.-M. Highly Porous Single Ion Conducting Membrane via a Facile Combined "Structural Self-Assembly" and in-situ Polymerization Process for High Performance Lithium Metal Batteries. *J. Membr. Sci.* **2021**, *636*, 119601. DOI: 10.1016/j.memsci.2021.119601.
(23) Chen, Y.; Li, C.; Ye, D.; Zhang, Y.; Bao, H.; Cheng, H. Lithiated Polyanion Supported $Li_{1.5}Al_{0.5}Ge_{1.5}(PO_4)_3$ Composite Membrane as Single-Ion Conducting Electrolyte for Security and Stability Advancement in Lithium Metal Batteries. *J. Membr. Sci.* **2021**, *620*, 118926. DOI: 10.1016/j.memsci.2020.118926.
(24) Chen, Y.; Ke, H.; Zeng, D.; Zhang, Y.; Sun, Y.; Cheng, H. Superior Polymer Backbone with Poly(arylene ether) over Polyamide for Single Ion Conducting Polymer Electrolytes. *J. Membr. Sci.* **2017**, *525*, 349–358. DOI: 10.1016/j.memsci.2016.12.011.
(25) Chen, Y.; Xu, G.; Liu, X.; Pan, Q.; Zhang, Y.; Zeng, D.; Sun, Y.; Ke, H.; Cheng, H. A Gel Single Ion Conducting Polymer Electrolyte Enables Durable and Safe Lithium Ion Batteries via Graft Polymerization. *RSC Adv.* **2018**, *8* (70), 39967–39975. DOI: 10.1039/C8RA07557C.
(26) Liang, H.-P.; Zarrabeitia, M.; Chen, Z.; Jovanovic, S.; Merz, S.; Granwehr, J.; Passerini, S.; Bresser, D. Polysiloxane-Based Single-Ion Conducting Polymer Blend Electrolyte Comprising Small-Molecule Organic Carbonates for High-Energy and High-Power Lithium-Metal Batteries. *Adv. Energy Mater.* **2022**, *3*, 2200013. DOI: 10.1002/aenm.202200013.
(27) Dong, X.; Mayer, A.; Liu, X.; Passerini, S.; Bresser, D. Single-Ion Conducting Multi-block Copolymer Electrolyte for Lithium-Metal Batteries with High Mass Loading NCM 811 Cathodes. *ACS Energy Lett.* **2023**, *8* (2), 1114–1121. DOI: 10.1021/acsenergylett.2c02806.
(28) Wang, Z.; Shen, L.; Deng, S.; Cui, P.; Yao, X. 10 μm-Thick High-Strength Solid Polymer Electrolytes with Excellent Interface Compatibility for Flexible All-Solid-State

Lithium-Metal Batteries. *Adv. Mater.* **2021**, *33* (25), e2100353. DOI: 10.1002/adma.202100353.
(29) Liu, Y.; Zhang, Y.; Pan, M.; Liu, X.; Li, C.; Sun, Y.; Zeng, D.; Cheng, H. A Mechanically Robust Porous Single Ion Conducting Electrolyte Membrane Fabricated via Self-Assembly. *J. Membr. Sci.* **2016**, *507*, 99–106. DOI: 10.1016/j.memsci.2016.02.002.
(30) Li, Z.; Lu, W.; Zhang, N.; Pan, Q.; Chen, Y.; Xu, G.; Zeng, D.; Zhang, Y.; Cai, W.; Yang, M.; Yang, Z.; Sun, Y.; Ke, H.; Cheng, H. Single Ion Conducting Lithium Sulfur Polymer Batteries with Improved Safety and Stability. *J. Mater. Chem. A* **2018**, *6* (29), 14330–14338. DOI: 10.1039/C8TA04619K.
(31) Wang, Z.; Guo, Q.; Jiang, R.; Deng, S.; Ma, J.; Cui, P.; Yao, X. Porous Poly(vinylidene fluoride) Supported Three-Dimensional Poly(ethylene glycol) Thin Solid Polymer Electrolyte for Flexible High Temperature All-Solid-State Lithium Metal Batteries. *Chem. Eng. J.* **2022**, *435*, 135106. DOI: 10.1016/j.cej.2022.135106.
(32) Borzutzki, K.; Dong, K.; Nair, J. R.; Wolff, B.; Hausen, F.; Eichel, R.-A.; Winter, M.; Manke, I.; Brunklaus, G. Lithium Deposition in Single-ion Conducting Polymer Electrolytes. *Cell Rep. Phys. Sci.* **2021**, *2* (7), 100496. DOI: 10.1016/j.xcrp.2021.100496.
(33) Miao, R.; Liu, B.; Zhu, Z.; Liu, Y.; Li, J.; Wang, X.; Li, Q. PVDF-HFP-based Porous Polymer Electrolyte Membranes for Lithium-Ion Batteries. *J. Power Sources* **2008**, *184* (2), 420–426. DOI: 10.1016/j.jpowsour.2008.03.045.
(34) Jiang, Z.; Carroll, B.; Abraham, K. M. Studies of some Poly(vinylidene fluoride) Electrolytes. *Electrochim. Acta* **1997**, *42* (17), 2667–2677. DOI: 10.1016/S0013-4686(97)00005-4.
(35) Krause, C. H.; Butzelaar, A. J.; Diddens, D.; Dong, D.; Théato, P.; Bedrov, D.; Hwang, B.-J.; Winter, M.; Brunklaus, G. Quasi-Solid Single Ion Conducting Polymer Electrolyte Membrane Containing Novel Fluorinated Poly(arylene ether sulfonimide) for Lithium Metal Batteries. *J. Power Sources* **2021**, *484*, 229267. DOI: 10.1016/j.jpowsour.2020.229267.
(36) Liaw, D.-J.; Chen, P.-S. Preparation and Properties of Polyesters Derived from 4,4'-Sulfonyl Dibenzoyl Chloride by Solution Polycondensation. *J. Polym. Sci. A Polym. Chem.* **1996**, *34* (5), 885–891. DOI: 10.1002/(SICI)1099-0518(19960415)34:5<885:AID-POLA17>3.0.CO;2-E.
(37) Chiou, M.-H.; Borzutzki, K.; Thienenkamp, J. H.; Mohrhardt, M.; Liu, K.-L.; Mereacre, V.; Binder, J. R.; Ehrenberg, H.; Winter, M.; Brunklaus, G. Durable Fast-Charging Lithium Metal Batteries Designed with Cross-Linked Polymer Electrolytes and Niobate-Coated Cathode. *J. Power Sources* **2022**, *538*, 231528. DOI: 10.1016/j.jpowsour.2022.231528.
(38) Borodin, O.; Smith, G. D. Development of Many-body Polarizable Force Fields for Li-Battery Components: 1. Ether, Alkane, and Carbonate-based Solvents. *J. Phys. Chem. B* **2006**, *110* (12), 6279–6292. DOI: 10.1021/jp055079e.
(39) Borodin, O.; Smith, G. D. Development of Many-body Polarizable Force Fields for Li-Battery Applications: 2. LiTFSI-doped Oligoether, Polyether, and Carbonate-based Electrolytes. *J. Phys. Chem. B* **2006**, *110* (12), 6293–6299. DOI: 10.1021/jp055080d.
(40) Borodin, O. Polarizable Force Field Development and Molecular Dynamics Simulations of Ionic Liquids. *J. Phys. Chem. B* **2009**, *113* (33), 11463–11478. DOI: 10.1021/jp905220k.
(41) Borzutzki, K.; Dong, D.; Wölke, C.; Kruteva, M.; Stellhorn, A.; Winter, M.; Bedrov, D.; Brunklaus, G. Small Groups, Big Impact: Eliminating Li^+ Traps in Single-Ion Conducting Polymer Electrolytes. *iScience* **2020**, *23* (8), 101417. DOI: 10.1016/j.isci.2020.101417.
(42) Chiou, M.-H.; Verweyen, E.; Diddens, D.; Wichmann, L.; Schmidt, C.; Neuhaus, K.; Choudhary, A.; Bedrov, D.; Winter, M.; Brunklaus, G. Selection of Polymer Segment Species Matters for Electrolyte Properties and Performance in Lithium Metal Batteries. *ACS Appl. Energy Mater.* **2023**, *6* (8), 4422–4436. DOI: 10.1021/acsaem.3c00571.

(43) Chen, Y.-H.; Hsieh, Y.-C.; Liu, K. L.; Wichmann, L.; Thienenkamp, J. H.; Choudhary, A.; Bedrov, D.; Winter, M.; Brunklaus, G. Green Polymer Electrolytes Based on Polycaprolactones for Solid-State High-Voltage Lithium Metal Batteries. *Macromol. Rapid Commun.* **2022**, *43* (20), e2200335. DOI: 10.1002/marc.202200335.
(44) Frenkel, D.; Smit, B. *Understanding Molecular Simulation*:*From Algorithms to Applications*, 2nd ed.; Computational science series, Vol. 1; Academic Press, 2002.
(45) Evans, D. J.; Holian, B. L. The Nose–Hoover Thermostat. *J. Chem. Phys.* **1985**, *83* (8), 4069–4074. DOI: 10.1063/1.449071.
(46) Palmer, B. J. Direct Application of Shake to the Velocity Verlet Algorithm. *J. Comput. Phys.* **1993**, *104* (2), 470–472. DOI: 10.1006/jcph.1993.1045.
(47) Martyna, G. J.; Tobias, D. J.; Klein, M. L. Constant Pressure Molecular Dynamics Algorithms. *J. Chem. Phys.* **1994**, *101* (5), 4177–4189. DOI: 10.1063/1.467468.
(48) Martyna, G. J.; Tuckerman, M. E.; Tobias, D. J.; Klein, M. L. Explicit Reversible Integrators for Extended Systems Dynamics. *Mol. Phys.* **1996**, *87* (5), 1117–1157. DOI: 10.1080/00268979600100761.
(49) Yeh, I.-C.; Berkowitz, M. L. Ewald Summation for Systems with Slab Geometry. *J. Chem. Phys.* **1999**, *111* (7), 3155–3162. DOI: 10.1063/1.479595.
(50) Evans, J.; Vincent, C. A.; Bruce, P. G. Electrochemical Measurement of Transference Numbers in Polymer Electrolytes. *Polymer* **1987**, *28* (13), 2324–2328. DOI: 10.1016/0032-3861(87)90394-6.
(51) Nölle, R.; Beltrop, K.; Holtstiege, F.; Kasnatscheew, J.; Placke, T.; Winter, M. A Reality Check and Tutorial on Electrochemical Characterization of Battery Cell Materials: How to Choose the Appropriate Cell Setup. *Mater. Today* **2019** (32), 131–146. DOI: 10.1016/j.mattod.2019.07.002.
(52) Fox, T. G.; Flory, P. J. Second-Order Transition Temperatures and Related Properties of Polystyrene. I. Influence of Molecular Weight. *J. Appl. Phys.* **1950**, *21* (6), 581–591. DOI: 10.1063/1.1699711.
(53) Fox, T. G.; Loshaek, S. Influence of Molecular Weight and Degree of Crosslinking on the Specific Volume and Glass Temperature of Polymers. *J. Polym. Sci.* **1955**, *15* (80), 371–390. DOI: 10.1002/pol.1955.120158006.
(54) Blanchard, L.-P.; Hesse, J.; Malhotra, S. L. Effect of Molecular Weight on Glass Transition by Differential Scanning Calorimetry. *Can. J. Chem.* **1974**, *52* (18), 3170–3175. DOI: 10.1139/v74-465.
(55) Pezzin, G.; Zilio-Grandi, F.; Sanmartin, P. The Dependence of the Glass Transition Temperature on Molecular Weight for Polyvinylchloride. *Eur. Polym. J.* **1970**, *6* (7), 1053–1061. DOI: 10.1016/0014-3057(70)90038-8.
(56) Flamme, B.; Rodriguez Garcia, G.; Weil, M.; Haddad, M.; Phansavath, P.; Ratovelomanana-Vidal, V.; Chagnes, A. Guidelines to Design Organic Electrolytes for Lithium-Ion Batteries: Environmental Impact, Physicochemical and Electrochemical Properties. *Green Chem.* **2017**, *19* (8), 1828–1849. DOI: 10.1039/c7gc00252a.
(57) Zhang, Y.; Rohan, R.; Cai, W.; Xu, G.; Sun, Y.; Lin, A.; Cheng, H. Influence of Chemical Microstructure of Single-Ion Polymeric Electrolyte Membranes on Performance of Lithium-Ion Batteries. *ACS Appl. Mater. Interfaces* **2014**, *6* (20), 17534–17542. DOI: 10.1021/am503152m.
(58) Dong, J.; Zhang, Y.; Wang, J.; Yang, Z.; Sun, Y.; Zeng, D.; Liu, Z.; Cheng, H. Highly Porous Single Ion Conducting Polymer Electrolyte for Advanced Lithium-Ion Batteries via Facile Water-induced Phase Separation Process. *J. Membr. Sci.* **2018**, *568*, 22–29. DOI: 10.1016/j.memsci.2018.09.052.

(59) Chen, Y.; Li, Z.; Liu, X.; Zeng, D.; Zhang, Y.; Sun, Y.; Ke, H.; Cheng, H. Construction of Interconnected Micropores in Poly(arylene ether) Based Single Ion Conducting Blend Polymer Membranes via Vapor-Induced Phase Separation. *J. Membr. Sci.* **2017**, *544*, 47–57. DOI: 10.1016/j.memsci.2017.09.003.
(60) Zhang, Y.; Lim, C. A.; Cai, W.; Rohan, R.; Xu, G.; Sun, Y.; Cheng, H. Design and Synthesis of a Single Ion Conducting Block Copolymer Electrolyte with Multifunctionality for Lithium Ion Batteries. *RSC Adv.* **2014**, *4* (83), 43857–43864. DOI: 10.1039/C4RA08709G.
(61) Chen, Y.; Tian, Y.; Li, Z.; Zhang, N.; Zeng, D.; Xu, G.; Zhang, Y.; Sun, Y.; Ke, H.; Cheng, H. An AB Alternating Diblock Single Ion Conducting Polymer Electrolyte Membrane for All-Solid-State Lithium Metal Secondary Batteries. *J. Membr. Sci.* **2018**, *566*, 181–189. DOI: 10.1016/j.memsci.2018.09.013.
(62) Borodin, O.; Smith, G. D. LiTFSI Structure and Transport in Ethylene Carbonate from Molecular Dynamics Simulations. *J. Phys. Chem. B* **2006**, *110* (10), 4971–4977. DOI: 10.1021/jp056249q.
(63) Stolz, L.; Hochstädt, S.; Röser, S.; Hansen, M. R.; Winter, M.; Kasnatscheew, J. Single-Ion versus Dual-Ion Conducting Electrolytes: The Relevance of Concentration Polarization in Solid-State Batteries. *ACS Appl. Mater. Interfaces* **2022**, *14* (9), 11559–11566. DOI: 10.1021/acsami.2c00084.
(64) Roering, P.; Overhoff, G. M.; Liu, K. L.; Winter, M.; Brunklaus, G. External Pressure in Polymer-Based Lithium Metal Batteries: An Often-Neglected Criterion When Evaluating Cycling Performance? *ACS Appl. Mater. Interfaces* **2024**, *16* (17), 21932–21942. DOI: 10.1021/acsami.4c02095. Published Online: Apr. 22, 2024.
(65) Zhang, X.; Kostecki, R.; Richardson, T. J.; Pugh, J. K.; Ross, P. N. Electrochemical and Infrared Studies of the Reduction of Organic Carbonates. *Electrochim. Acta* **2001**, *148* (12), A1341. DOI: 10.1149/1.1415547.
(66) Borzutzki, K.; Nair, J. R.; Winter, M.; Brunklaus, G. Does Cell Polarization Matter in Single-Ion Conducting Electrolytes? *ACS Appl. Mater. Interfaces* **2022**, *14* (4), 5211–5222. DOI: 10.1021/acsami.1c19097.
(67) Wang, C.; Yu, R.; Hwang, S.; Liang, J.; Li, X.; Zhao, C.; Sun, Y.; Wang, J.; Holmes, N.; Li, R.; Huang, H.; Zhao, S.; Zhang, L.; Lu, S.; Su, D.; Sun, X. Single Crystal Cathodes Enabling High-Performance All-Solid-State Lithium-Ion Batteries. *Energy Storage Mater.* **2020**, *30*, 98–103. DOI: 10.1016/j.ensm.2020.05.007.
(68) Yi, M.; Li, J.; Fan, X.; Bai, M.; Zhang, Z.; Hong, B.; Zhang, Z.; Hu, G.; Jiang, H.; Lai, Y. Single Crystal Ni-rich Layered Cathodes Enabling Superior Performance in All-Solid-State Batteries with PEO-based Solid Electrolytes. *J. Mater. Chem. A* **2021**, *9* (31), 16787–16797. DOI: 10.1039/d1ta04476a.
(69) Han, Y.; Jung, S. H.; Kwak, H.; Jun, S.; Kwak, H. H.; Lee, J. H.; Hong, S.-T.; Jung, Y. S. Single- or Poly-Crystalline Ni-Rich Layered Cathode, Sulfide or Halide Solid Electrolyte: Which Will be the Winners for All-Solid-State Batteries? *Adv. Energy Mater.* **2021**, *11* (21), 2100126. DOI: 10.1002/aenm.202100126.
(70) Borzutzki, K.; Winter, M.; Brunklaus, G. Improving the NMC111|Polymer Electrolyte Interface by Cathode Composition and Processing. *J. Electrochem. Soc.* **2020**, *167* (7), 70546. DOI: 10.1149/1945-7111/ab7fb5.
(71) Overhoff, G. M.; Ali, M. Y.; Brinkmann, J.-P.; Lennartz, P.; Orthner, H.; Hammad, M.; Wiggers, H.; Winter, M.; Brunklaus, G. Ceramic-in-Polymer Hybrid Electrolytes with Enhanced Electrochemical Performance. *ACS Appl. Mater. Interfaces* **2022**, *14* (48), 53636–53647. DOI: 10.1021/acsami.2c13408.

Graphical Abstract (TOC)